Drainage-induced control of avalanches in foam coalescence

Alesya Mikhailovskaya, Cécile Monteux

Drainage-induced control of avalanches in foam coalescence†

Alesya Mikhailovskaya[a] and Cécile Monteux*[a,b]

Surfactant foams are particularly unstable because of avalanches of coalescence which lead to an instant collapse of considerable part of the foam volume when the liquid fraction falls below a critical value. In many applications it is crucial to control the occurence of these avalanches phenomena. In this study we compare the evolution of a foam made from a surfactant solution with a foam stabilized by a surface-active polymer and show that avalanches phenomena can be suppressed for the polymer stabilized foams for which a coalescence front slowly propagates between the top to the bottom of the foam. We demonstrate that the occurence and length-scale of avalanches is controlled by the liquid fraction profile in the foams which is set by the rate of drainage. Our study therefore illustrates the strong coupling between drainage and coalescence and provides means to control it by varying the type of foam stabilizer used.

Introduction

Liquid foams are concentrated dispersions of gas bubbles in a solution containing surface active agents required to stabilize the liquid-gas interfaces. The liquid fraction $\phi = V_{liquid}/V_{foam}$ in foams is usually small, so that the bubbles get in contact and deform into a polyhedral shape to achieve a dense structure. In this packing, bubbles are separated by thin liquid films that meet each other in liquid channels, so called Plateau borders (PBs), that are in turn connected in nodes. Such interconnected soft structure of liquid films and channels has a very high surface-to-volume ratio which makes foams indispensable in many industrial processes and in personal life products[1,2].

Foams are thermodynamically unstable and tend to disappear because of three main destabilization mechanisms[3]. *Coarsening* occurs because of the gas diffusion from smaller bubbles to bigger ones due to the difference in Laplace pressure. *Drainage*, due to gravity, leads to very thin films which are more likely to rupture, leading to *coalescence* of bubbles. These mechanisms, especially coarsening and drainage, are strongly interrelated[4–7] and foam structure is evolving under their action in a continuous manner. However, when ϕ becomes very low, a film rupture can initiate an abrupt foam collapse due to avalanche of coalescence events over which hundreds of bubbles break in a short time[8,9].

The mechanism of coalescence avalanches remains debated[10,11]. A first scenario suggests that for very dry foams the capillary pressure in the system reaches a critical value that overcomes the critical disjoining pressure that the isolated thin liquid films can sustain without breaking[12,13]. However, different authors also report that coalescence occurs in foams with film thicknesses well above and capillary pressures well below the critical values[14,15]. Another set of studies considered dynamical processes in evolving foams[14,15] and relates film rupture with bubble rearrangements events, known as T1 processes, which occur during foam aging and consists in switching of the neighbours between the bubbles. As sketched in Figure 1, a T1 transition proceeds with the shrinkage of the film which separates initially adjacent bubbles, followed by the pulling of a fresh film from a created liquid node. Carrier and Colin demonstrated the existence of a critical liquid fraction ϕ^* below which the foams collapse, which decreases with the surfactant concentration[14]. They suggested that for insufficient surfactant concentrations the surfactant adsorption time becomes larger than the T1 duration time, τ, hence the surfactant molecules do not have time to stabilize the fresh films generated during the T1, resulting in an abrupt foam collapse. Biance et al. used a hydrodynamic approach to describe the coalescence avalanches and associated ϕ^* with the amount of liquid that is necessary to withdraw a new film[15]. Below a critical liquid fraction, the amount of liquid in the Plateau borders is insufficient to allow a T1 rearrangement. Besides their model used the fact that the dilatational viscosity of the surfactant layers, κ, controls the T1 duration time $\tau \approx \kappa/\gamma$ hence the velocity at which a fresh film is pulled from the nodes. This pulling velocity controls hydrodynamically the thickness of the fresh films and subsequently the amount of liquid needed to allow for the creation of the fresh film and the critical liquid fraction. A third scenario assumes that foam collapse is a stochastic process which depends on the bubble surface area[16–18].

To control the stability of a foam it is necessary to regulate the occurrence and length scale of these avalanches phenomena. In this work we explore the coupling between the avalanche phenomenon and the drainage flow. We show that catastrophic coalescence avalanches, which are observed for a standard non ionic surfactants, can be suppressed by using very low concentrations of amphiphilic polymer. We demonstrate that the length scale of avalanches is related to the liquid fraction profile in foams, which is controled by the drainage velocity.

[a] *Sciences et Ingénierie de la Matiére Molle, ESPCI Paris, PSL Research University, CNRS, Sorbonne Universités, UPMC Univ Paris 06, 75005 Paris, France. Tel: +33 (0)1 4079 4745; E-mail: cecile.monteux@espci.fr*

[b] *Global Station for Soft Matter, Global Institution for Collaborative Research and Education, Hokkaido University, Sapporo, Japan..*

† Electronic Supplementary Information (ESI) available: [details of any supplementary information available should be included here]. See DOI: 10.1039/cXsm00000x/

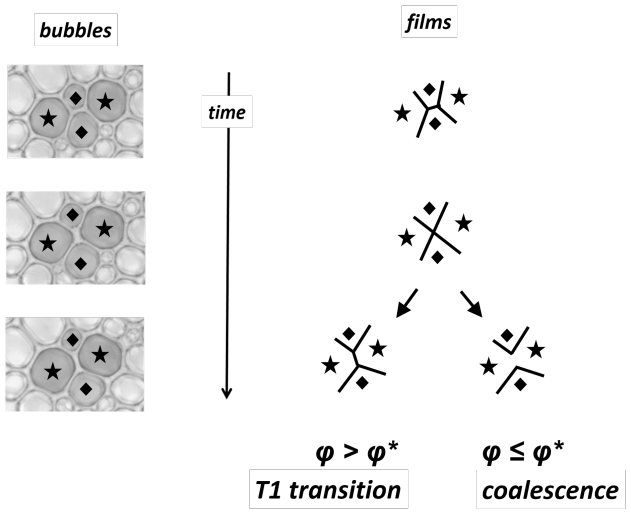

Fig. 1 *Left*: Topological transition T1 that occurs in a cluster of two pairs of neighbouring bubbles noted with star and diamond symbols. *Right*: Sketch of film rearrangement during the transition and possible final situations.

Experimental section

Amphiphilic molecules

We use a non-ionic surfactant, BrijO10 purchased from Sigma-Aldrich and an amphiphilic polymer, a partially hydrolyzed Polyvinyl (alcohol), PVA, (Mowiol 8-88, $M_W = 51$ kg/mol from Sigma-Aldrich), containing 88% of vinyl alcohol monomers and 12% of vinylacetate monomers. The concentrations of foaming solutions (20 mM for BrijO10 and 0.1wt% for PVA) are chosen in a way that the amount of surface active elements is the same for both systems, considering the fraction of acetate groups in PVA macromolecules that provide surface activity of the polymer. Since BrijO10 and PVA do not carry any charge we add 20 mM of sodium chloride into all foaming solutions to improve their conductivity response for the experiments on the liquid fraction evolution.

Dynamic surface properties

We measured the dynamic surface tension $\gamma(t)$ using automated tensiometer TRACKER (Teclis-scientific) in the configuration of rising bubble. The experiments lasted 5 hours in respect that the dynamics of polymer adsorption is rather slow.

We obtain dilatational surface modulus E by measuring the variation of interfacial tension during oscillation of interfacial bubble area A at a frequency f of 0.1 Hz and a surface deformation amplitude of 3%, with $E = d\gamma \Big/ dA$. The dilatational surface elasticity refers to the real part of the complex modulus $E = E' + iE''$ oscillating the bubble and the dilatational surface viscosity is related to the imaginary part as $\kappa = E'' \Big/ 2\pi f$.

Bulk viscosity

We measured viscosity of foaming solution using a AR-G2 Rheometer (TA Instruments) in a cone-plate geometry with the cone angle 2°, diameter 40 mm, truncation 52 mm. We performed frequency sweeps in the range of 5-1000 Hz to ensure the Newtonian behaviour of the foaming solutions.

All measurements are made at 25 °C, and with a solvent trap to avoid evaporation.

Foam preparation

To create the foams, air is forced through a porous frit that is localized at the bottom of an acrylic cell (250 mm height, 30 mm x 30 mm square cross section) covered by 50 ml of solution. During the experiment the acrylic cell is sealed on the top to avoid the evaporation.

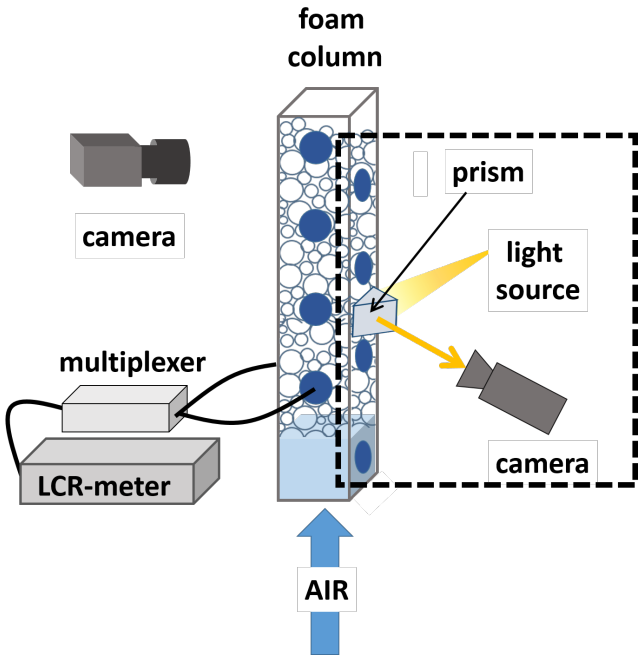

Fig. 2 Experimental setup: a plexiglass cell has 8 pairs of electrodes, each of them is connected to the LCR-meter equipped by a multiplexer, a camera takes picture to follow the evolution of the foam height. Dashed zone: imaging of the bubbles at the cell surface is due to camera which takes pictures through a prism.

The initial bubble radius R_b^{init} is controlled by the size of the pores and most of the experiments are performed with $R_b^{init} = 75$ μm. We measure R_b^{init} straight after their formation by imaging a thin layer of foam using a microscope[19].

Foaming lasts until the bubbles fill the cell from bottom to top. We take this moment as a zero age of a studied foam.

Measurement of liquid fraction evolution

We obtain ϕ values from the foam electrical conductivity[20] measured by pairs of circular electrodes which have the radius of 4 mm and located at various positions along the cell height. The electrodes are connected to an impedance meter (LCR Meter, Chroma 11021) operating at a frequency of 1kHz and at voltage 1V. The apparatus measures the resistance of a parallel resistor–capacitor equivalent circuit, the value which is reciprocal to conductivity. Simultaneously we observe the foam height using a

camera. The setup is sketched in Figure 2.

Foam imaging at the wall of the column

During the ageing of the foam we take pictures of the bubbles at the surface of the measuring cell trough a prism attached to the cell wall (see the dashed zone in Figure 2. Using an open source image processing program ImageJ, we determine surface area A_b of bubbles and we convert it into the bubble radii $R_{b,surf} = \sqrt{A_b/\pi}$. The value $R_{b,surf}(0)$ corresponds to the zero time. The Sauter mean radius $\langle R_{b,surf}\rangle = \sum_{i=1}^{n} n_i R_{b,surf}^3 / \sum_{i=1}^{n} n_i R_{b,surf}^2$ averaged over n bubbles at the image increases during the foam ageing. Since the size of the analyzed image is restricted by the perimeter of the prism, n decreases with time. We perform the analysis until the number of bubbles becomes less than 100.

The image analysis allows us also to determine the surface liquid fraction ϕ_s at the foam height of the prism and recalculate it into the volume liquid fraction ϕ as[21] $\phi = \phi_c(1-\sqrt{1-\phi_s})^2$, where ϕ_c is the limit value at which bubbles come apart and remain spherical.

Results and Discussion

We explore the propagation of coalescence avalanches in foams with different drainage rate but similar ϕ^*. For this purpose we compare the ageing of foams stabilized either with a non-ionic surfactant BrijO10 or with an amphiphilic polymer, a partially hydrolyzed PVA which presents a slow rate of drainage[22]. Both systems present the similar values of bulk viscosity and interfacial tension and they demonstrate negligible dilatational surface viscosity as we summarize in Table 1. Therefore according to Biance et al.[15] we expect the critical liquid fraction to be identical for both systems. Moreover, for both solutions the concentration in amphiphilic moities was chosen to be the same and the dynamic surface tension drops immediately after the creation of air/liquid interface (ESI). Thus, we assure that the reservoir of amphiphilic moieties in the films is similar for both systems[14].

The foaming process lasts several minutes and hence proceeds simultaneously with the drainage of the continuous phase in the created foam column. Therefore we observe a gradient of the liquid fraction along the foam height at early times in the experiment (Figure 3a). Surfactant-stabilized foam has a steep profile of ϕ with a very dry foam on the top and most of the liquid collected on the bottom of the cell. Reduced drainage in PVA-stabilized foam results in a wetter foam at the top, which liquid fraction increases smoothly as the height decreases.

At longer times, the liquid fraction continuously decreases due to drainage without any change in the foam height. For BrijO10, the foam collapses when the liquid fraction approaches $\phi^*_{BrijO10} = 0.0005$. Thousands of bubbles break and the surface of electrodes is no more covered by the foam. At this moment registered signal abruptly drops at a given height as it is shown in Figure 3c. Carrier and Collin[14] observed similar behaviour for foams stabilized by common surfactants and the reported value of ϕ^* is in agreement with our data.

In the case of the polymer-stabilized foam (Figure 3c) coalescence proceeds in a more gradual manner over a total duration of 2000 seconds, as bubbles burst layer by layer, starting from the top of the column. As the foam front reaches the position of an electrode, its surface becomes covered only partially reducing the measured value. As a result, the time-dependency of the liquid fraction represents a continuous decrease with a change in the curve slope that occurs at the moment of the foam front arrival and hence there is no intermittence in the liquid fraction evolution, as we show in Figure 3c. The plateau values measured at the late stages of both experiments is due to conductivity of the wetting films at the surface of the cell.

Table 1 Stabilizer type, surface tension γ, the surface dilatational elasticity E' and viscosity κ measured by the oscillating bubble method at a frequency of $f = 0.1Hz$ and a surface deformation amplitude of 3%, and bulk viscosity η for the foaming solutions used in the experiments.

Stabilizer	γ, mN/m	E', mN/m	κ, mN·s/m	η, mPa·s
PVA	49.1	10.1	5.1	1.1
BrijO10	31.3	1.2	7.0	1.4

We assume that the reason of the difference in the length-scale of the coalescence avalanches in two foams originates from the difference in the liquid fraction profiles that are developed in the foams under drainage of different rate. In Figure 3b we present the distributions of the liquid fraction that correspond to the last moment before BrijO10-stabilized foam collapses and for the PVA foam of the same age. Fast drainage in the first case leads to a development of an almost vertical ϕ profile during the foam ageing. The main part of the curve lays in the region of ϕ^* that sets the limit of the foam stability. Therefore, in the next moment the avalanches affect a considerable fraction of the foam volume leading to an abrupt drop of the foam height. At the same age, the foam stabilized by PVA is much wetter at the level of each electrode and the liquid distribution is more gradual due to the reduced drainage. Apparently, the size of electrodes does not allow to resolve the liquid profile on the very top of the foam column where we expect to have the largest gradient of the liquid fraction with height. We speculate that in this case the portion of the foam that is under critical condition corresponds roughly to a layer of bubbles, which burst gradually leading to a slow decrease of the foam height. Therefore, the foam vanishing is less catastrophic.

To verify our assumption, we perform an experiment of forced drainage which enables us to obtain a PVA foam with a low liquid fraction that is homogeneously distributed along the foam height. The foaming solution is continuously added at the top of the foam and evacuated at its bottom with the same flow rate which determines the liquid fraction. We then stop the forced drainage and let the foam age on its own. As we show in Figure 4a, we are able to set a steep initial liquid fraction profile in the PVA-stabilized foam which is similar to the one which BrijO10-foam has just before the propagation of avalanches starts. In Figure 4b we plot the time evolution of liquid fraction at a given position in the foam column. We note that the liquid fraction profile remains steep over time and that the liquid fraction does not depend on the height (not shown). We observe an avalanche of coalescence that gives a drop in $\phi(t)$-dependence. Foam collapse in this case re-

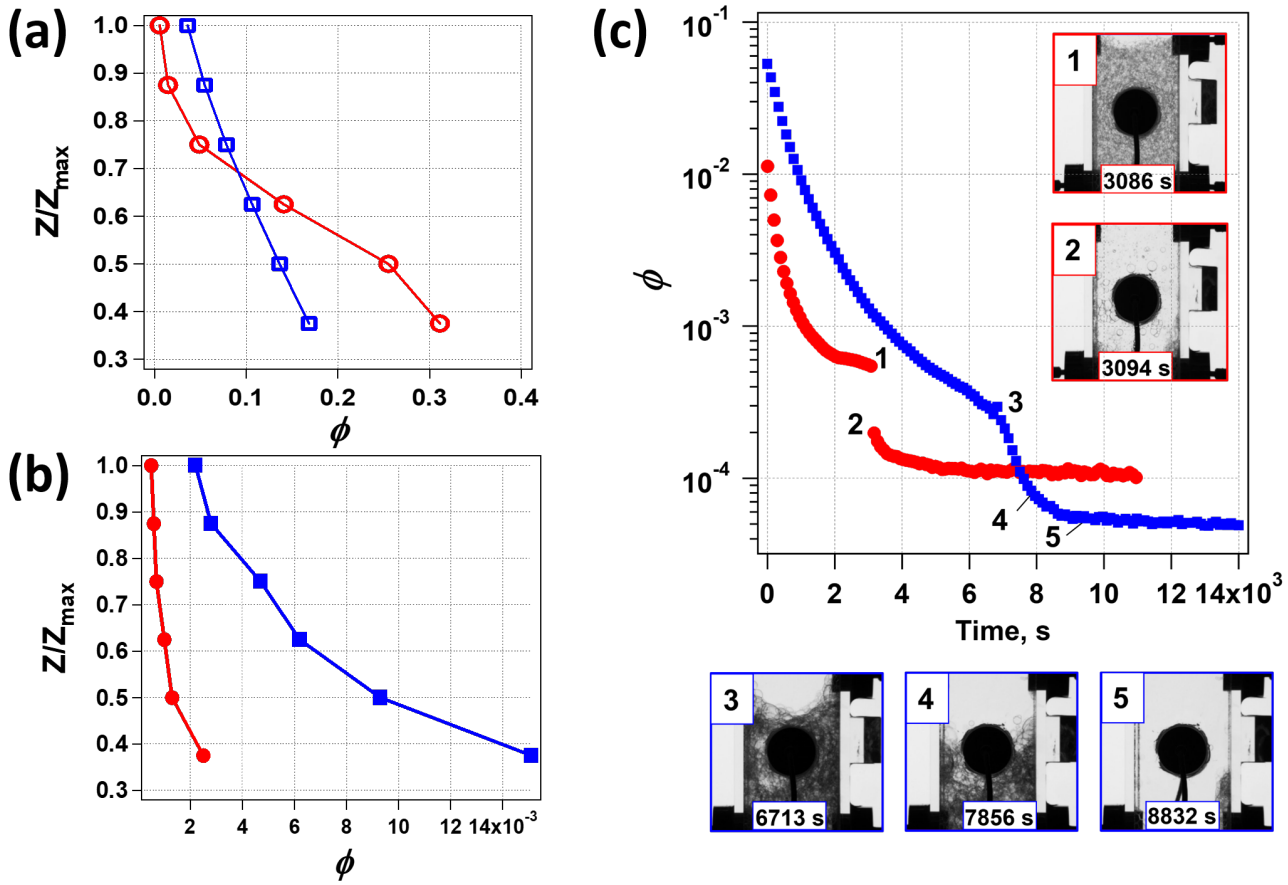

Fig. 3 Distribution of the liquid fraction along the normalized foam height in of a foam stabilized by 20 mM of Brij O10 (red circles) and of a foam stabilized by 0.1wt% of PVA (blue squares) at (a) the initial stage of foam life-time (empty symbols) and (b) before occurrence of coalescence avalanches (filled symbols). Lines are guides for the eye. (c) Evolution of the liquid fraction at a given pair of electrodes ($Z/Z_{max} = 0.875$) for a foam stabilized by 20 mM of BrijO10 (red circles) and of a foam stabilized by 0.1wt% of PVA (blue squares). Numbered photos illustrate the corresponding points at the curves.

peats the scenario of a BrijO10 foam: the liquid fraction initially decreases due to natural drainage and when ϕ^* is approached it abruptly drops because of avalanches of coalescence events. We can also clearly see that avalanches occur at a liquid fraction close to $\phi^*_{BrijO10}$ as we presumed in the beginning. Thus, we demonstrate that the length-scale of the coalescence avalanches is primarily governed by the liquid fraction profile in the foam. To ensure that PVA foam collapses under the same critical condition regardless the bubble size, we perform the same forced drainage experiment with a different initial bubble radius, $R_b^{init} = 100\ \mu$m. The critical liquid fraction is the same as for both formerly studied foams indicating its indifference to the bubble size. This is in line with experimental results obtained with surfactants[14,15,23], the same, however, had never been proven for polymer-stabilized foams.

Even though we do not observe coalescence avalanches in PVA-stabilized foams in spontaneous drainage experiments, we observe single bubble coalescence events in the middle of the foam column. We reveal their occurrence with the analysis of the average bubble size evolution from the images taken at the surface of the cell. The corresponding curves are shown in Figure 5. The presented values $\langle R_{b,surf} \rangle$ do not correspond directly to the size of the bubbles in the bulk of the foam[24], but they give an idea on the rate of the bubble size evolution[25]. In the case of BrijO10, we observe an induction period which is determined by the initial polydispersity of bubble size[3], after which the average radius $\langle R^{BrijO10}_{b,surf} \rangle$ increases linearly with the square root of the foam age, which is characteristic for the coarsening of dry foams[26–28]. However in the case of the PVA-stabilized foams $\langle R^{PVA}_{b,surf} \rangle$ presents a faster increase which can only be explained by individual bubble coalescence in addition to the coarsening. However these individual coalescence events have no crucial influence on the avalanches character: they do not initiate a collective film rupture in the bulk of the foam and the main coalescence front still propagates from the top to the bottom of the foam column. Our results therefore demonstrate that the dynamics of bubble coalescence strongly depends on the type of stabilizer used : for the PVA stabilized foams, bubble coalescence occurs in an isolated manner while in surfactant foams bubble break in a collective manner in avalanches.

Conclusions

By comparing foams stabilized either by a surfactant or a surface active polymer, in which coalescence occurs under similar critical

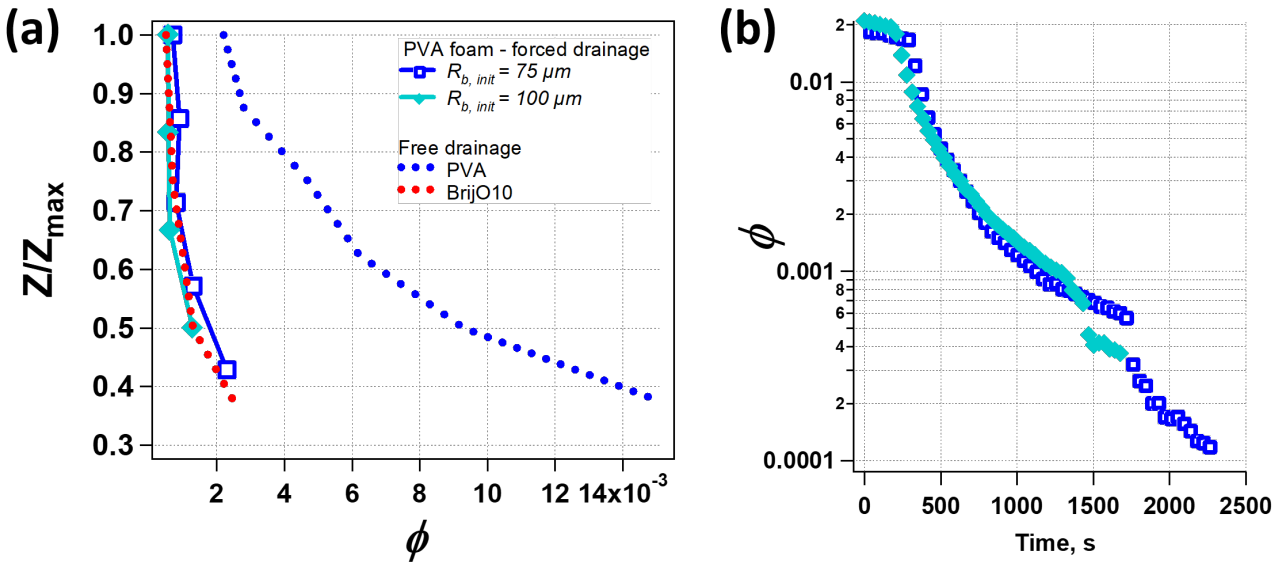

Fig. 4 Liquid fraction in the PVA-stabilized foam prepared using forced drainage technique: a) height profile for the foams with $R_b^{init} = 75\mu m$ (blue empty squares) and with $R_b^{init} = 100\mu m$ (cyan filled diamonds). The profiles for the foams with free drainage are replotted from Figure 3b and shown with dashed lines; b) time evolution for the PVA foam with $R_b^{init} = 75\mu m$ at the level of $Z/Z_{max} = 0.85$ (blue empty squares); for the $R_b^{init} = 100\mu m$ at the level of $Z/Z_{max} = 0.67$ (cyan diamonds). Lines are guides for the eyes.

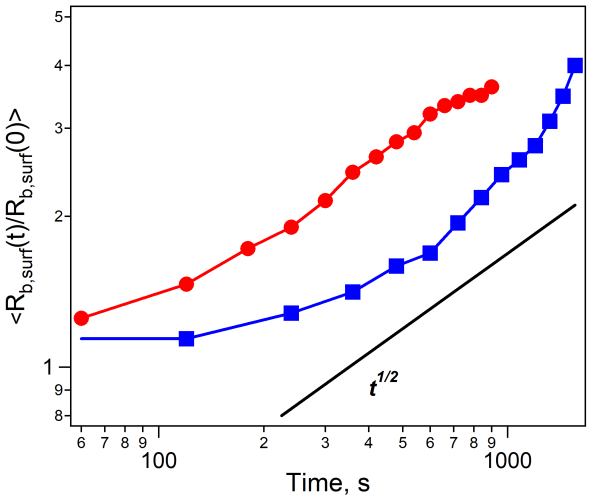

Fig. 5 Relative increase of the average bubble radius measured at the surface of the measuring cell for the foam stabilized by BrijO10 (red circles) and PVA (blue squares). Filled symbols correspond to foams with $R_b^{init} = 75\mu m$ and empty symbols correspond to $R_b^{init} = 100\mu m$. The black solid line has the slope of $t^{1/2}$, where t is time. Lines are guides for the eyes. The error bars depend on the threshold which is used to transform the image into a binary one and they are within the size of the used symbols.

conditions but which differ by the drainage flow, we show that the length-scale of foam collapse is governed by the distribution of the liquid fraction over the foam height. In the case of the surfactant foam, the liquid fraction profile is steep and the foam is homogeneously dry. When ϕ^* is approached a collective rupture of bubbles in large avalanches proceeds. For the polymer-stabilized foams, for which the liquid fraction profile evolves more gradually with the foam height, the avalanches are suppressed and a coalescence front slowly propagates from the top to the bottom of the foam. In conclusion, our study demonstrates the strong coupling between drainage and coalescence and provides means to control and suppress avalanches phenomena by varying the type of stabilizer used.

Conflicts of interest

There are no conflicts to declare.

Acknowledgements

We acknowledge the technical support of Jérémie Sanchez, Vincent Klein, Ludovic Olanier and Alexandre Lantheaume and fruitful discussions with Nadège Pantoustier and Patrick Perrin. This work was financially supported by ANR FOAMEX grant number ANR-17-CE08-0016.

Notes and references

1 P. Stevenson, *Foam engineering: fundamentals and applications*, John Wiley & Sons, 2012.
2 C. Hill and J. Eastoe, *Advances in Colloid and Interface Science*, 2017, **247**, 496–513.
3 I. Cantat, S. Cohen-Addad, F. Elias, F. Graner, R. Höhler, O. Pitois, F. Rouyer and A. Saint-Jalmes, *Foams: Structure and Dynamics*, Oxford University Press, 2013.
4 S. Hilgenfeldt, S. A. Koehler and H. A. Stone, *Physical review letters*, 2001, **86**, 4704.
5 A. Saint-Jalmes and D. Langevin, *Journal of Physics: Condensed Matter*, 2002, **14**, 9397.
6 A. Saint-Jalmes, *Soft Matter*, 2006, **2**, 836–849.
7 E. Rio and A.-L. Biance, *ChemPhysChem*, 2014, **15**, 3692–3707.

8 W. Müller and J. Di Meglio, *Journal of Physics: Condensed Matter*, 1999, **11**, L209.
9 N. Vandewalle, H. Caps and S. Dorbolo, *Physica A: Statistical Mechanics and its Applications*, 2002, **314**, 320–324.
10 A. Colin, *Foam Engineering: Fundamentals and Applications, edited by: Stevenson, P., John Wiley & Sons, Ltd., Chichester, UK*, 2012, 75–90.
11 E. Rio and D. Langevin, *Encyclopedia of Surface and Colloid Science*, 2012.
12 J. Bibette, D. C. Morse, T. Witten and D. Weitz, *Physical review letters*, 1992, **69**, 2439.
13 K. Khristov, D. Exerowa and G. Minkov, *Colloids and Surfaces A: Physicochemical and Engineering Aspects*, 2002, **210**, 159–166.
14 V. Carrier and A. Colin, *Langmuir*, 2003, **19**, 4535–4538.
15 A. L. Biance, A. Delbos and O. Pitois, *Physical Review Letters*, 2011, **106**, 1–4.
16 D. Georgieva, A. Cagna and D. Langevin, *Soft Matter*, 2009, **5**, 2063–2071.
17 S. Tobin, A. Meagher, B. Bulfin, M. Möbius and S. Hutzler, *American Journal of Physics*, 2011, **79**, 819–824.
18 E. Forel, B. Dollet, D. Langevin and E. Rio, *Physical review letters*, 2019, **122**, 088002.
19 T. Gaillard, C. Honorez, M. Jumeau, F. Elias and W. Drenckhan, *Colloids and Surfaces A: Physicochemical and Engineering Aspects*, 2015, **473**, 68–74.
20 K. Feitosa, S. Marze, A. Saint-Jalmes and D. J. Durian, *Journal of Physics Condensed Matter*, 2005, **17**, 6301–6305.
21 E. Forel, E. Rio, M. Schneider, S. Beguin, D. Weaire, S. Hutzler and W. Drenckhan, *Soft Matter*, 2016, **12**, 8025–8029.
22 R. Deleurence, T. Saison, F. Lequeux and C. Monteux, *Soft Matter*, 2015, **11**, 7032–7037.
23 E. Carey and C. Stubenrauch, *Journal of Colloid and Interface Science*, 2010, **346**, 414–423.
24 Y. Wang and S. J. Neethling, *Colloids and Surfaces A: Physicochemical and Engineering Aspects*, 2009, **339**, 73–81.
25 A. E. Roth, B. G. Chen and D. J. Durian, *Physical Review E - Statistical, Nonlinear, and Soft Matter Physics*, 2013, **88**, 1–9.
26 D. Durian, D. Weitz and D. Pine, *Science*, 1991, **252**, 686–688.
27 J. A. Glazier and D. Weaire, *Journal of Physics: Condensed Matter*, 1992, **4**, 1867.
28 N. Isert, G. Maret and C. M. Aegerter, *The European Physical Journal E*, 2013, **36**, 116.